Tuning the Nanotopography and Chemical Functionality of 3D Printed Scaffolds through Cellulose Nanocrystal Coatings

Babi, Mouhanad; Riesco, Roberto; Boyer, Louisa; Fatona, Ayodele; Accardo, Angelo; Malaquin, Laurent; Moran-Mirabal, Jose

DOI
10.1021/acsabm.1c00970

Publication date
2021

Document Version
Final published version

Published in
ACS Applied Bio Materials

ACS APPLIED BIO MATERIALS

www.acsabm.org Article

Tuning the Nanotopography and Chemical Functionality of 3D Printed Scaffolds through Cellulose Nanocrystal Coatings

Mouhanad Babi, Roberto Riesco, Louisa Boyer, Ayodele Fatona, Angelo Accardo, Laurent Malaquin, and Jose Moran-Mirabal*

Cite This: *ACS Appl. Bio Mater.* 2021, 4, 8443–8455 Read Online

ACCESS | Metrics & More | Article Recommendations | Supporting Information

ABSTRACT: In nature, cells exist in three-dimensional (3D) microenvironments with topography, stiffness, surface chemistry, and biological factors that strongly dictate their phenotype and behavior. The cellular microenvironment is an organized structure or scaffold that, together with the cells that live within it, make up living tissue. To mimic these systems and understand how the different properties of a scaffold, such as adhesion, proliferation, or function, influence cell behavior, we need to be able to fabricate cellular microenvironments with tunable properties. In this work, the nanotopography and functionality of scaffolds for cell culture were modified by coating 3D printed materials (DS3000 and poly(ethylene glycol)diacrylate, PEG-DA) with cellulose nanocrystals (CNCs). This general approach was demonstrated on a variety of structures designed to incorporate macro- and microscale features fabricated using photopolymerization and 3D printing techniques. Atomic force microscopy was used to characterize the CNC coatings and showed the ability to tune their density and in turn the surface nanoroughness from isolated nanoparticles to dense surface coverage. The ability to tune the density of CNCs on 3D printed structures could be leveraged to control the attachment and morphology of prostate cancer cells. It was also possible to introduce functionalization onto the surface of these scaffolds, either by directly coating them with CNCs grafted with the functionality of interest or with a more general approach of functionalizing the CNCs after coating using biotin−streptavidin coupling. The ability to carefully tune the nanostructure and functionalization of different 3D-printable materials is a step forward to creating *in vitro* scaffolds that mimic the nanoscale features of natural microenvironments, which are key to understanding their impact on cells and developing artificial tissues.

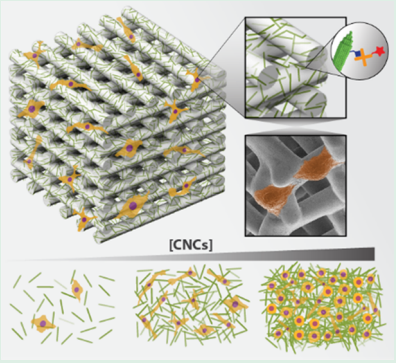

KEYWORDS: *bioprinting, additive manufacturing, cell culture, mechanobiology, biomimetic, cell microenvironment*

1. INTRODUCTION

Recent advances in three-dimensional (3D) printing technologies and biomaterials have given rise to a variety of scaffold designs and compositions designed to mimic natural microenvironments and culture cells *in vitro*. Examples of this include the fabrication of artificial bone grafts through fused deposition modeling of calcium phosphate and collagen composites, extrusion-photopolymerization printing of poly(ethylene glycol)diacrylate (PEG-DA)/alginate hydrogel composites, and electrohydrodynamic jet printing of polycaprolactone/poly(vinylpyrrolidone) scaffolds.[1−3] In addition to incorporating a variety of complex geometrical features, these materials present a broad range of mechanical, physical, and chemical properties. These differences reflect the desire to mimic cellular niches that are found within the various types of tissues that make up multicellular organisms. While artificial scaffolds are effective in producing bulk 3D structures to encapsulate and support cells, they often still require tuning and functionalization to mimic the extracellular matrix (ECM) features found in real tissues. Micro- to nanoscale features of the ECM, such as topography, stiffness, and decoration with various biochemical motifs play an important role in the proliferation, migration, differentiation, and overall function of the cell.[4] Thus, whether to understand the role of the ECM on cellular behavior, study cells in their native environment, or create artificial tissues, it is important to fabricate 3D cellular scaffolds with properties similar to those of tissues.

The *in vivo* extracellular environment possesses nanoscale structures and topography that play a key role in determining the behavior and function of cells both in healthy and diseased tissues. The main structural component of tissue, the ECM, provides biochemical and mechanical support to cells by virtue of a fibrous network, primarily composed of proteins like collagen and elastin that possesses nanoscale dimensions and introduces nanotopography in the cellular microenvironment.

Received: September 9, 2021
Accepted: November 9, 2021
Published: November 17, 2021

https://doi.org/10.1021/acsabm.1c00970
ACS Appl. Bio Mater. 2021, 4, 8443−8455

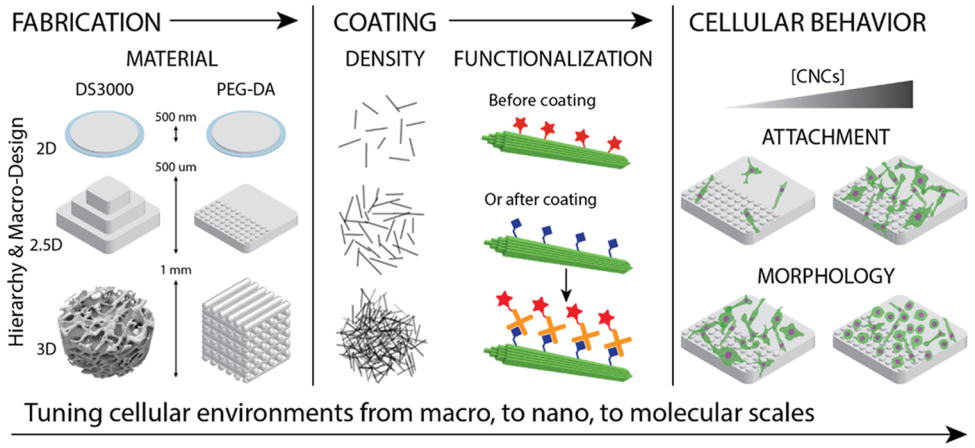

Figure 1. Fabrication of cellular microenvironments with tunable nanotopography and functionality. Spin-coating (followed by flood exposure to UV-light) and one- or two-photon 3D printing were used to fabricate scaffolds of increasing complexity, ranging from 2D thin films to 2.5D and 3D structures. The topography of these scaffolds can be finely tuned by the LbL deposition of a coating of CNCs with densities spanning from sparse to dense coverage of the surface. Using chemically modified CNCs, the scaffold surface can be functionalized during coating with a moiety of interest (red star in the schematic) that is directly grafted on the CNC surface, or after coating with a molecule that targets the functionality encoded on the coated CNCs. Careful tuning of the CNC coating density on the 3D printed scaffolds permits control of cell adhesion and phenotype.

This fibrous network provides structural and mechanical cues that direct cellular adhesion, morphology, migration, and differentiation.[5−7] For instance, collagen fibrils, which have a width of 20−200 nm and a periodic ridged structure with 67 nm spacing and 5−15 nm grooves, present nanostructures that cells interact with through integrin-mediated focal or 3D matrix adhesions.[8−10] Through these contact points, the alignment of collagen fibrils has been shown to guide the migration of fibroblast, epithelial, and carcinoma cells within the 3D matrix.[11−13] *In vivo* substratum nanotopography can also be found in endothelial and corneal epithelium basement membranes, which present a 3D fibrous texture rich in nanoscale (20−200 nm) pores and ridges that are vital for cellular adhesion and act as the foundation of large-scale multicellular architectures including tissues and organs.[14−16] Given the ubiquitous presence and importance of nanoscale topography *in vivo*, the incorporation of surface nanostructures and roughness during the fabrication of artificial microenvironments is key to promoting relevant behavior and function of cells cultured *in vitro*.

Nanostructured surfaces can be made through various fabrication and patterning techniques and have been previously shown to modulate cellular behavior. Ordered and regular nanoscale features, such as nanopillars, nanogrooves, and nanopits, can be produced using colloidal, electron beam, or soft lithography.[17−19] Solely from the anisotropic topography presented by nanogrooves (320−2100 nm wide), human corneal cells elongate and align themselves with the pattern, and in the case of human embryonic stem cells, also differentiate into neuronal lineages without the use of any biochemical differentiation factors.[18,19] Electrospinning of synthetic or natural polymers can be used to create highly porous 3D networks of fibers with controllable widths and pores at the submicron scale and have been used to study human ligament fibroblast alignment and proliferation.[20] In a benchtop fabrication approach, thermoresponsive substrates can be used to wrinkle thin films to produce micro/nanostructured surfaces. Silicon dioxide thin films structured through this method were shown to alter the morphology of murine macrophages into star-shaped cells that displayed enhanced phagocytic abilities.[21]

Incorporating nanoscale structures in artificial scaffolds can play a pivotal role in controlling cell phenotype. However, despite the abundance of nanostructuring techniques, they are often limited to transforming flat surfaces into more complex 2.5D structures or 3D scaffolds with limited depth. While these structures are a significant improvement over commonly used two-dimensional (2D) cell culture dishes, they still fall short in recapitulating the nanotopography present within the 3D environment of biological systems.

Light-assisted 3D printing techniques have become an attractive route for the fabrication of cell and tissue culture scaffolds. These techniques use inks containing photosensitive resins and initiators that result in cross-linking when exposed to light either through a projected image or a scanned laser source. By translating the sample or the source of illumination, a 3D structure can be printed layer-by-layer (LbL) or voxel-by-voxel. This additive manufacturing technology allows the fabrication of scaffolds with complex architectures and precisely defined geometries from the macro- to the microscopic scale. While the resolution offered by light-assisted 3D printing is superior to those of other 3D printing techniques, the natural diffraction of light limits its resolution to ∼200 nm and prevents nanoscale features from being printed onto scaffolds for cell culture.[22] As a result, 3D printed scaffolds are often smooth and require subsequent modifications to incorporate surface nanotopography.

A way to incorporate nanotopography on the surface of 3D scaffolds is to dope the bulk material with nanoparticles (NPs). The high surface-area-to-volume ratio of NPs makes them easily dispersible and ideal to blend with other materials through bulk mixing or surface coating. Attractive properties of NPs, such as piezoelectricity (TiO_2), magnetism (Fe_3O_4), conductivity (carbon nanotubes), antimicrobial effects (Ag), and biodegradability (nanocellulose) can be imparted to the scaffold with the added benefit of mechanical reinforcement. For example, the antioxidant properties of polydopamine/puerarin nanoparticles have been shown to enhance the wound healing properties of PEG-DA-based hydrogel materials.[23] The dimensions of NPs also increase the roughness of scaffolds and have been shown to modify the way cells interact with them. The incorporation of

https://doi.org/10.1021/acsabm.1c00970
ACS Appl. Bio Mater. 2021, 4, 8443−8455

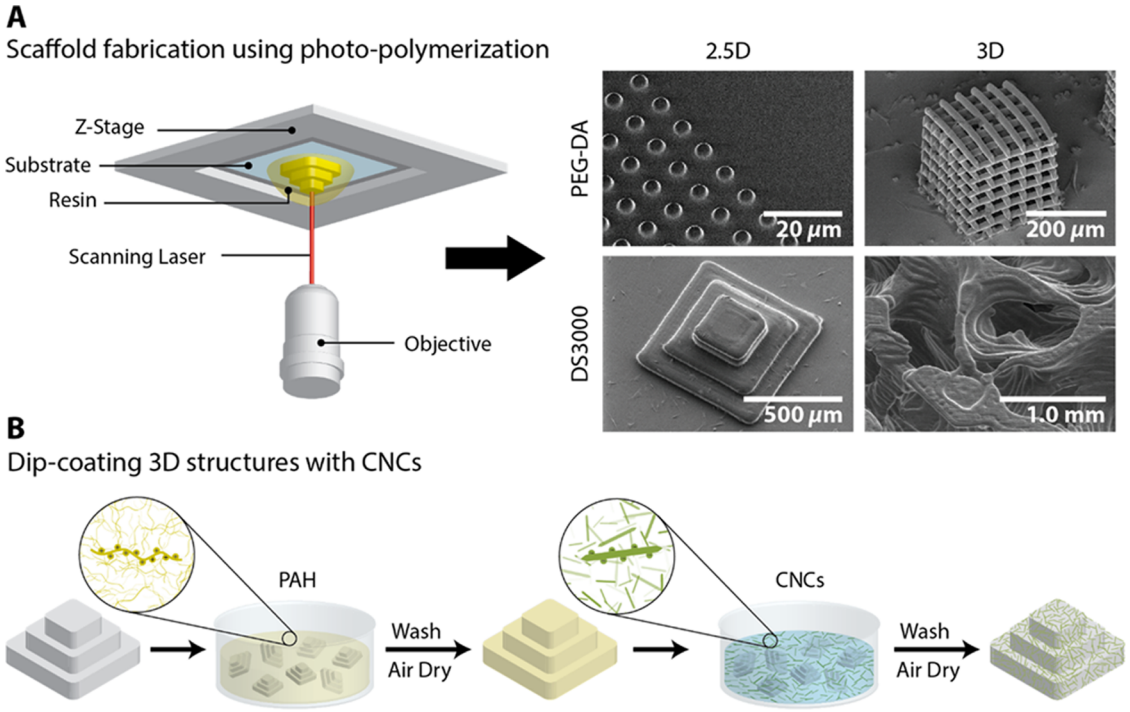

Figure 2. Three-dimensional (3D) printing and dip coating of scaffolds. (A) 2.5D and 3D structures made of DS3000 and PEG-DA were fabricated using single-photon and two-photon polymerization 3D printing, respectively. This technique involves a moveable laser source that polymerizes the resin and prints the structure in a layer-by-layer fashion. (B) Two-dimensional (2D) thin films and 3D printed structures were coated with CNCs using a LbL dip-coating approach, which uses the linear cationic polymer poly(allylamine hydrochloride) (PAH) as an adhesive layer to bind anionic CNCs to the surface of the structures.

carbon nanotubes, poly(lactic-*co*-glycolic acid), hydroxyapatite, and silica nanoparticles within 3D scaffolds has been shown to enhance the adhesion and proliferation of stem cells and promote their differentiation to adipogenic, osteogenic, and neurogenic lineages.[24−28] Yet, in most cases the NPs are incorporated within the bulk material before or during fabrication of the 3D scaffolds, which limits their availability on the surface and can significantly change the bulk mechanical properties of the whole scaffold.[29] Another challenge for their incorporation into 3D printing inks is that NPs can introduce significant light scattering that hinders the photopolymerization of the inks. Given the difficulty in modifying the surface roughness of 3D printed scaffolds, it is not surprising that few studies have quantitatively characterized the nanotopography of composite scaffolds or its impact on cellular adhesion and morphology. A simple method of modifying the surface of 3D printed scaffolds through NP coatings could thus significantly aid in the study of how nanotopography can control the behavior of cells cultured in artificial 3D microenvironments.

In this work, we develop a simple and versatile method (Figure 1) for tuning the nanotopography and functionality of 3D printed scaffolds via dip coating with cellulose nanocrystals (CNCs). CNCs are rod-shaped, rigid, and highly crystalline nanoparticles produced from cellulosic materials through strong acid hydrolysis.[30] CNCs have typical lengths of 100−200 nm and widths of 5−20 nm[31] and exhibit excellent mechanical properties, and high thermal and chemical stability.[32] The abundant hydroxyl groups present on the surface of CNCs can be used to graft small molecules or polymers, endowing them with targeted functionalities; to this end, a variety of surface modification approaches have been reported in the literature.[33−36] Their intrinsic physicochemical properties, non-cytotoxicity, biodegradability (primarily by fungal and bacterial enzymes), and low production cost are advantages that have made CNCs attractive materials to incorporate into *in vitro* scaffolds for applications in tissue engineering and regenerative medicine.[37,38]

We have leveraged the intrinsic surface charge of CNCs to coat 3D printed structures via a layer-by-layer (LbL) dip-coating approach, which relies on a cationic polymer to electrostatically bind CNCs to the surface.[39] Such a LbL method has been previously used to coat 2D surfaces to produce thin CNC films for biosensing, optical, drug delivery, and controlled adhesion applications but to our knowledge has not been used to coat 3D structures or to confer nanotopography and modulate cellular behavior.[40] Our simple and versatile approach is demonstrated on thin films, 2.5D and 3D structures fabricated from commercially available resins using photopolymerization and 3D printing. We showcase the ability to tune the nanoscale roughness and coating density on the 3D printed scaffolds by characterizing the coatings through atomic force microscopy (AFM) and confocal microscopy. The ability to functionalize 3D printed scaffolds with chemically modified CNCs is also shown using two approaches: (i) precoating functionalization, where the moiety of interest is first grafted onto CNCs and then the functionality is transferred to the scaffold surface during coating; (ii) postcoating functionalization, where the scaffold is first coated with functional CNCs and then a second molecule of interest is specifically bound to the CNCs on the scaffold surface. The impact of CNC coatings and their density on the adhesion and morphology of PC3 prostate cancer cells is evaluated to understand how tuneable nanoscale roughness and surface chemistry can be used to influence cell phenotype. We anticipate that this simple method for tuning the nanotopography and

https://doi.org/10.1021/acsabm.1c00970
ACS Appl. Bio Mater. 2021, 4, 8443−8455

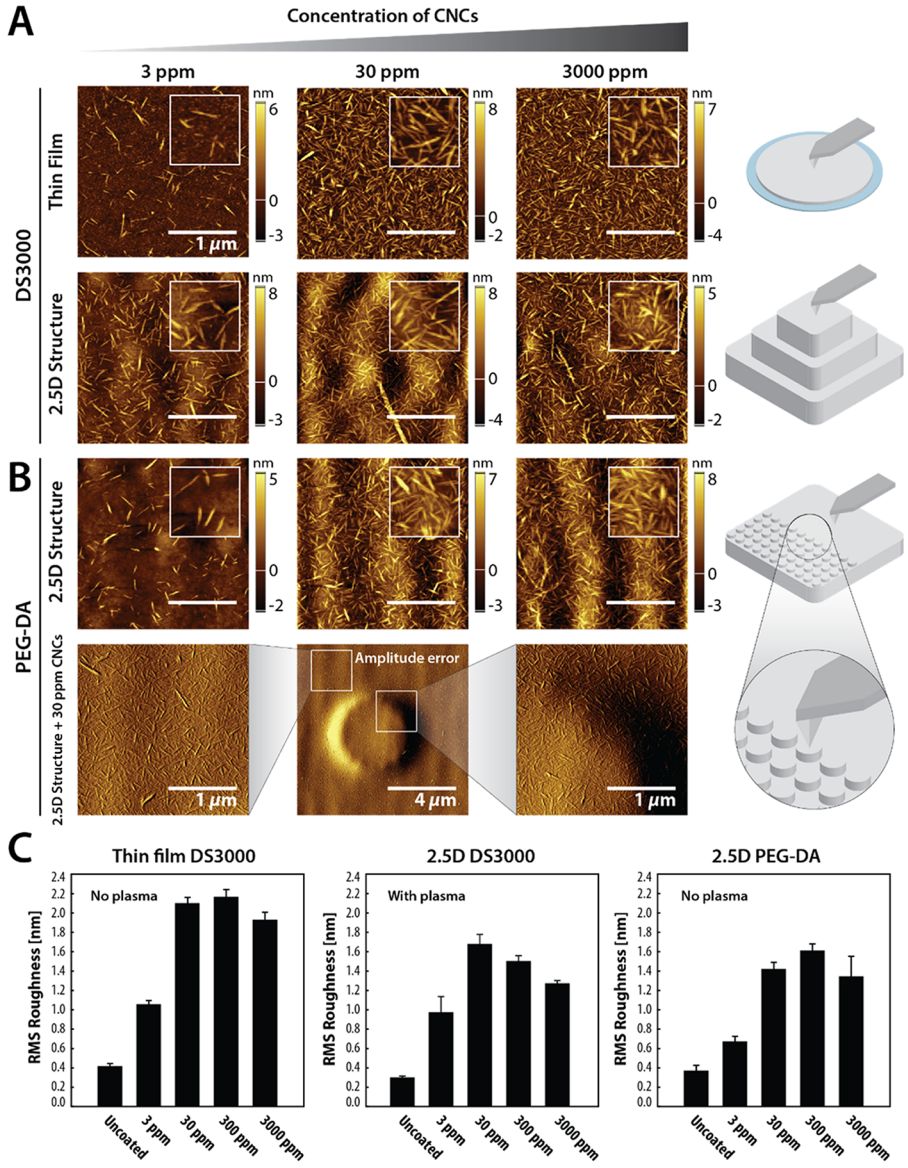

Figure 3. Characterization of the CNC coating density using AFM. (A, B) 2D thin films and 3D printed 2.5D structures made from PEG-DA or DS3000 were coated with CNCs using suspensions with concentrations of 3, 30, 300, and 3000 ppm. As opposed to the DS3000 pyramid, the DS3000 thin-film and PEG-DA pillars were not activated with plasma before coating. The resulting surface density and RMS roughness were characterized by AFM, in three different areas of the thin film, the top surface of the DS3000 pyramid, or the flat half of PEG-DA pillar structures. The image insets are a 0.5 μm × 0.5 μm portion of the image. An amplitude error map of a scan of the PEG-DA pillar was generated to highlight the ability to uniformly coat the wall and top surfaces of 3D printed structures. (C) RMS roughness was calculated from at least three images, and in the case of 2.5D structures, polynomial background subtraction of the underlying large order topography was performed beforehand.

functionality of 3D printed scaffolds will aid in the development of biomimetic cellular microenvironments for applications in tissue engineering and regenerative medicine.

2. RESULTS AND DISCUSSION

2.1. Fabrication of Cellular Scaffolds via 3D Printing.

To investigate the ability of the LbL method to coat 3D printed structures with CNCs, scaffolds of various sizes and geometrical complexities were fabricated using two commercially available photosensitive materials with contrasting properties: (i) PEG-DA, a polymeric material that is hydrophilic, protein-repellent, and relatively soft (under the fabrication conditions and fully hydrated) and (ii) DS3000, a material that is hydrophobic, protein-binding, and mechanically stiff. DS3000 was 3D printed using a single-photon polymerization stereolithography printer (DWS 028J+, DWS Systems, Italy), which allowed the rapid fabrication of centimeter size structures, with feature sizes down to 30−40 μm.[41] On the other hand, a two-photon polymerization (2PP) 3D printing system (Photonic Professional GT, Nanoscribe, Germany) was used to fabricate PEG-DA structures with submicron resolution but was limited to sub-millimeter sized designs. PEG-DA scaffolds were printed on glass substrates spin-coated with a thin film of DS3000 to improve adhesion.[42] Thin films of PEG-DA and DS3000 were also used as flat, 2D surfaces to accurately characterize CNC coatings with AFM. This surface characterization was extended to simple 2.5D structures that had planar facets compatible with AFM imaging, which included a 300 μm × 300 μm × 15 μm base of PEG-DA half-covered with 5 μm diameter, 5 μm high pillars, or DS3000 square pyramids with 700, 500, and 300 μm bases (Figure 2A).

https://doi.org/10.1021/acsabm.1c00970
ACS Appl. Bio Mater. 2021, 4, 8443−8455

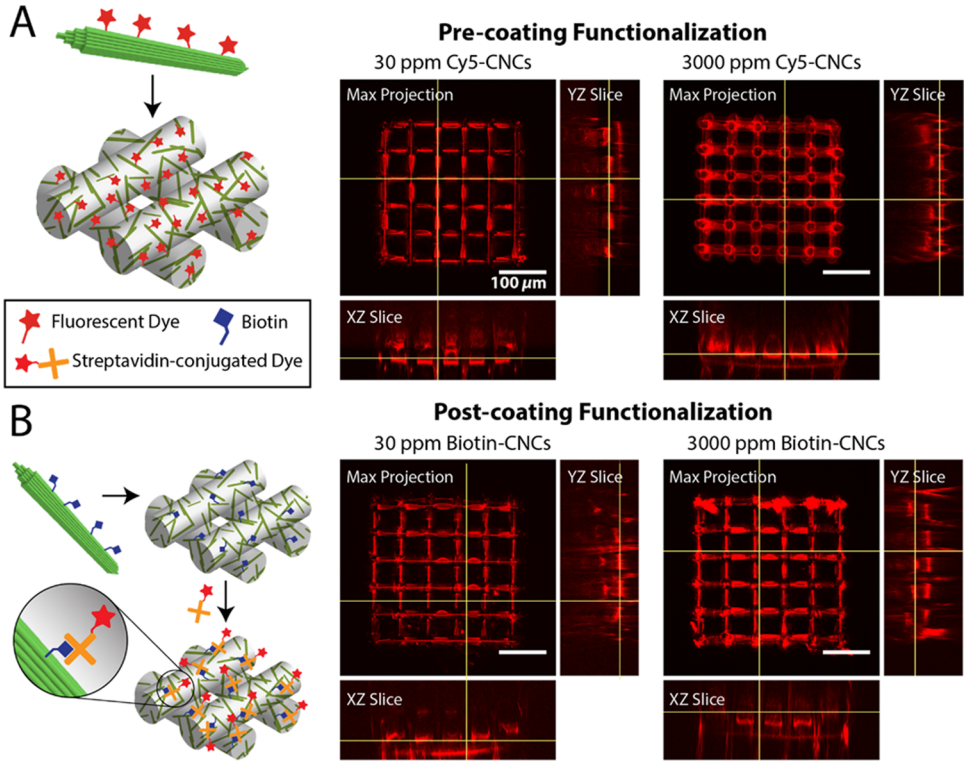

Figure 4. Coating and functionalization of 3D PEG-DA woodpiles with chemically modified CNCs. The ability to functionalize 3D printed PEG-DA structures through (A) precoating functionalization or (B) postcoating functionalization of CNCs was evaluated using the Cy5 dye as a reporter and was characterized using laser scanning confocal microscopy. Fluorescence *z*-stack images were acquired in the far-red channel with a slice thickness of 1.2 μm and a total depth of 180 μm. *XY* images were obtained using a maximum sum projection of the stack while *YZ* and *XZ* orthogonal projections were single slices taken at the positions indicated by the yellow lines.

The coating was then tested on 3D structures that contained overhanging features, such as the 270 μm × 270 μm × 270 μm PEG-DA woodpile and a complex, centimeter-sized DS3000 scaffold with a design reconstructed from 3D tomography of a horse trabecular bone. Thus, 2D, 2.5D, and 3D structures with macroscopic and microscopic features were fabricated from PEG-DA and DS3000 through photopolymerization and 3D printing and were subsequently used to study the ability to coat these scaffolds with CNCs.

2.2. Tunable Surface Coating of 3D Printed Scaffolds with CNCs. Thin-films and 3D printed structures made from DS3000 and PEG-DA were coated with CNCs using the LbL dip coating method. Because of the hydrophobic character of the DS3000 samples, samples with 2.5D and 3D structures were first activated with air plasma to increase the surface wettability and avoid the formation of air pockets that could decrease the coating efficiency. The samples were then immersed in a bath containing PAH, a linear polycation, which adsorbed onto the surface and introduced positive charges (Figure 2B). After washing away excess PAH, the structures were placed into a bath containing a suspension of CNCs, which electrostatically bound to the PAH adhesive layer and effectively coated the scaffold surface. The importance of the PAH layer in coating surfaces with CNCs can be seen by the lack of nanoparticles adsorbed on bare PEG-DA thin films even when a high concentration of CNCs was used (Figure S1A). Furthermore, a two-step washing of the PAH-coated structures was essential to remove the excess or loosely bound polymer and obtain uniform and reproducible coatings (Figure S1C,D). When using low CNC concentrations, inadequate removal of excess PAH through a single washing step resulted in nonuniform coatings with large areas that were devoid of CNCs and the presence of CNC aggregates; similarly, when using high CNC coating concentrations, incomplete PAH washing led to the formation of a dense, fibrillated cellulose film (Figures S1A and S2A). In the case of 3D PEG-DA woodpile structures, incomplete washing of PAH also caused clogging, webbing, and bridging of the scaffolds with cellulose films (Figure S1E). By thoroughly washing excess PAH, it was possible to reproducibly coat thin films and 3D printed structures with various concentrations of CNCs.

AFM was used to characterize the surface of coated thin films and 2.5D structures, where the coating density and surface roughness were evaluated as a function of plasma activation and the CNC concentration used during the coating process. For DS3000 thin films coated without plasma activation and a low CNC concentration (3 ppm), the surface was sparsely covered with individual CNCs, and the root mean square (RMS) surface roughness increased from 0.4 to 1.0 nm (Figure 3A,B). At a 10-fold higher concentration of 30 ppm, the coating density significantly increased and yielded a connected network of CNCs with a roughness of 2.1 nm. This effect leveled off at higher CNC concentrations, with more complete coverage of the thin film and a maximum roughness of 2.2 nm (at 300 ppm CNCs) and a slight decrease to 1.8 nm when a 3000 ppm CNC solution was used. The decrease in RMS roughness at the highest concentration is attributed to the formation of a complete CNC layer where the roughness is no longer dictated by the difference in height between the diameter of the nanoparticles and the surface but by the packing between the CNCs themselves, as evidenced by line scans obtained from AFM measurements (Figure S2B). The coating of PEG-DA thin films yielded similar results with low concentrations resulting in

https://doi.org/10.1021/acsabm.1c00970
ACS Appl. Bio Mater. 2021, 4, 8443−8455

sparse coatings and high concentrations leading to complete surface coverage with CNCs (Figure S2C).

The dip-coating approach also allowed the controlled deposition of CNC coatings with tunable density on structures made through 3D printing from DS3000 and PEG-DA inks (Figure 3A,B). Unlike spin-coated flat films, which had an RMS roughness of 0.4 nm (Figure S1A), the surface of 2.5D structures presented intrinsic inhomogeneous topographies either from the 3D printing process or caused by drying and wrinkling. Thus, the RMS roughness of uncoated surfaces varied from 0.5 to 4.0 nm, making it necessary to perform a polynomial background subtraction to determine the roughness introduced solely by the CNC coating (Figure S3A). Surprisingly, the observed roughness of coated 2.5D structures was lower than that of thin films (Figure 3C). This can be seen when comparing the height profiles of CNCs imaged on a DS3000 thin film, which were 4−6 nm high, to those on a PEG-DA 2.5D structure, which had a height of 2−4 nm (Figure S3B). The observed discrepancy is attributed to the inability of the AFM to map the full height of CNCs when they are overlaid on large-scale topography and to over smoothing by the polynomial fit. The coating efficiency, as visualized from the density of surface-bound CNCs, was similar for both thin films and the PEG-DA 2.5D structures. However, the 2.5D DS3000 pyramid was coated more efficiently, which can be seen by the higher coating density when a dilute CNC solution of 3 ppm was used. This can be explained by the activation of the surface with plasma, which introduces negative surface charges and enhances the adsorption of the positively charged PAH polymer chains. The higher coating efficiency introduced by plasma activation caused the maximum roughness and complete coverage of the surface to occur at more dilute CNC concentrations (Figure 3C). Finally, to demonstrate the ability of this method to uniformly coat microscale features, an AFM scan was acquired from a 5 μm diameter PEG-DA pillar that was coated using a 30 ppm CNC suspension (Figure 3B, bottom row). Through the amplitude error map, it is possible to see homogeneous coverage by CNCs across the base, walls, and top surfaces of the pillar. Altogether, these results show that the dip-coating process allows easy tuning of the roughness and density of CNCs on thin films and 3D printed structures made from DS3000 and PEG-DA by simply changing the CNC concentration used.

2.3. Functionalization of 3D Printed Scaffolds with Chemically Modified CNCs. The use of chemically modified CNCs opens the door to a simple route for the functionalization of 3D printed scaffolds via dip coating. Through chemical derivatization of CNCs, functionalities of interest can be grafted onto the nanoparticle surface and introduced onto the scaffolds using two strategies: (i) precoating functionalization, where the moiety of interest is first grafted onto the CNC and then transferred to the scaffold surface during coating or (ii) postcoating functionalization, amenable to biomolecules sensitive to drying, where the scaffold is first coated with CNCs grafted with a binding group and then a second molecule of interest is specifically targeted to the CNCs containing the binding group on the scaffold surface (Figure 4). The precoating functionalization was demonstrated by coating the PEG-DA woodpile and DS3000 bone 3D scaffolds with CNCs grafted with the far-red dye Cy5, which allowed their visualization with laser scanning confocal microscopy. With as little as 30 ppm CNCs, 10% of which were grafted with the Cy5 dye, the PEG-DA woodpile scaffold displayed a fluorescent coating (Figures 4A and S4A). At a higher concentration of 3000 ppm CNCs, the full surface of the beams was easily visible in the orthogonal projections and 3D rendering (Figures 4A and S4A) of confocal microscopy images. Coating a trabecular bone scaffold, made from DS3000 resin, with Cy5-CNCs allowed the visualization of the highly complex architecture of the reconstructed bone and demonstrated the ability to coat and functionalize small, free-standing features within the structure (Figure S4B) using as little as a 3 ppm suspension of Cy5-CNCs. However, due to the heterogeneity in features presented by the scaffold, it was not possible to consistently visualize similar areas within individual prints and study the impact of CNC concentrations or other conditions on coating.

The postcoating functionalization approach was demonstrated by first coating the scaffolds with CNCs, 10% of which had biotin grafted onto their surface, and then incubating the coated scaffolds with a solution containing Cy5-labeled streptavidin. Functionalization of the structures after coating with Cy5-streptavidin yielded fluorescence images like those obtained with the prefunctionalization approach (Figure 4B) but with a ∼4× lower fluorescence intensity. This was attributed to differences in the degree of functionalization of the CNCs and streptavidin with Cy5. With both functionalization scenarios, it was only possible to visualize the first two layers of the woodpile structure due to limitations to how deep the confocal laser could penetrate (typically 40 μm) and how much of the emitted fluorescence could be recorded. However, in cases where the scaffolds were partially detached from the glass substrate, it was possible to acquire an image of the tilted structure and visualize the outer beams of the whole woodpile, which confirmed that the CNC coating was uniform across the whole structure (Figure S3B). Using chemically modified CNCs, it was possible to functionalize 3D scaffolds with Cy5 dyes either through direct functionalization of the CNCs or streptavidin−biotin coupling. The latter strategy is amenable to a variety of commercially available functionalities that are biologically relevant but sensitive to drying, such as structural proteins, enzymes, receptors, and differentiation factors which are key members of cellular microenvironments found in tissues. Functionalization through this route would preserve the native structure and activity of these biochemical factors that otherwise might not survive the steps involved in directly grafting them to CNCs or coating the scaffolds with the nanoparticles.

The LbL dip-coating method has been previously used for the fabrication of multilayered, nanostructured composite biomaterials that consist of CNCs, polyelectrolyte, and other scaffolding polymers like collagen, chitosan, and poly(oligoethyleneglycol-methacrylate).[43−45] While this method has been traditionally used for creating thin films or 2.5D structures, we have demonstrated that this approach can be extended to coat 3D printed scaffolds with tunable densities of CNCs. We have also observed that these coatings remain on the structures for several months under hydrated conditions and for years when stored under dry conditions, highlighting their excellent stability. The ability to coat both DS3000 and PEG-DA, which possess contrasting physical and chemical properties, suggests that this method can be applied to other biomaterials commonly used in 3D printing to confer nanotopography and functionalization. The versatility of this approach stems from the ability of PAH to nonspecifically interact with various charged and uncharged materials, as we observed that the introduction of surface negative charges through plasma treatment was not necessary to achieve coating. The interactions between the

https://doi.org/10.1021/acsabm.1c00970
ACS Appl. Bio Mater. 2021, 4, 8443−8455

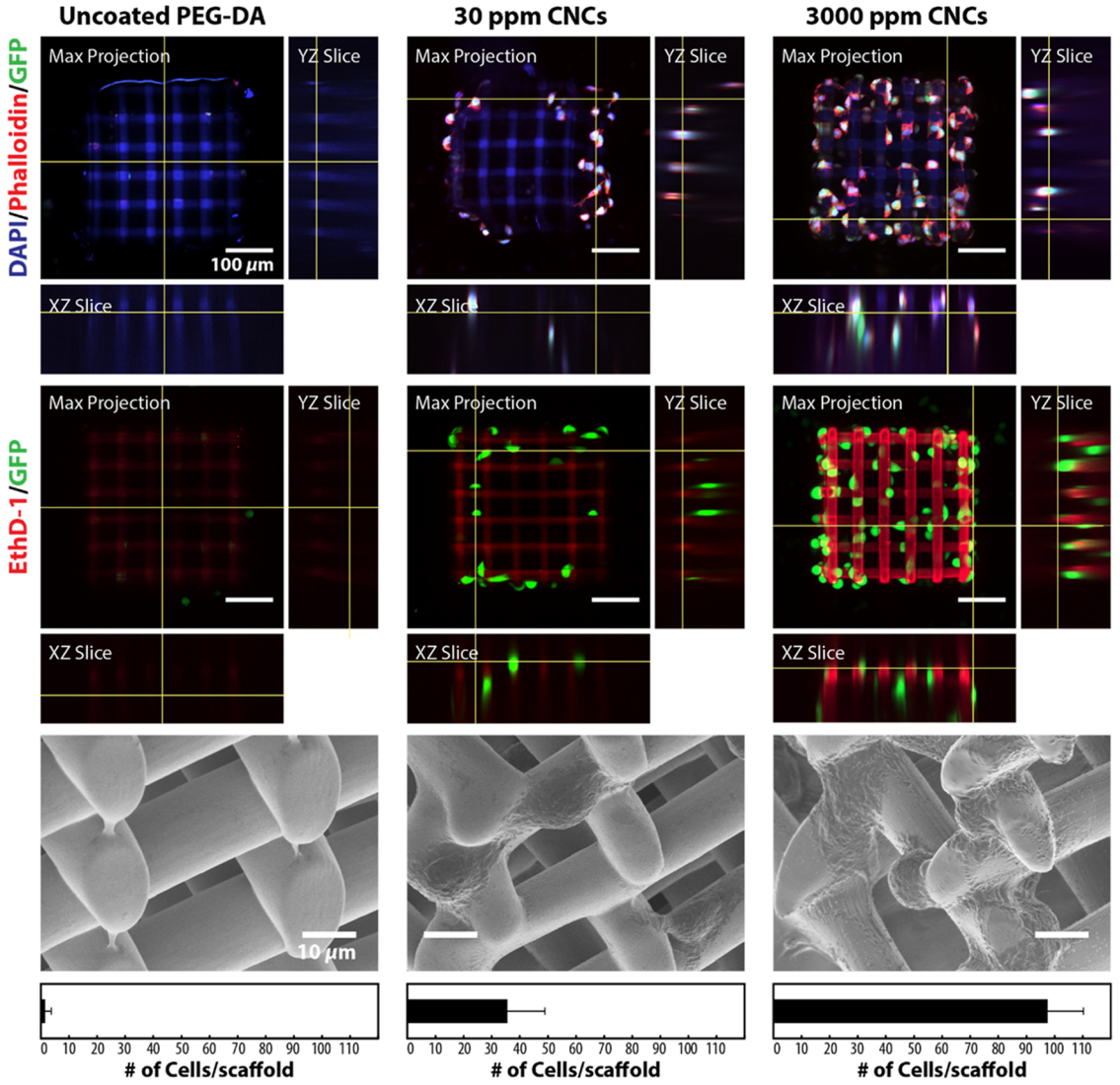

Figure 5. The adhesion of PC3-GFP prostate cells to PEG-DA 3D woodpile structures could be tuned by the density of CNC coatings. PC3-GFP prostate cancer cells, which constitutively expressed green fluorescence protein (GFP) in the cytoplasm, were seeded on the PEG-DA scaffolds at a density of 10 000 cells/cm^2 for 1 h, supplemented with media, and cultured for 2 days. Images in the top row are of formalin-fixed cells stained for the nucleus and actin filaments using 4′,6-diamidino-2-phenylindole (DAPI) and rhodamine−phalloidin, respectively, and were acquired using spinning-disk confocal microscopy. The cells in the second row were cultured under the same conditions and stained with ethidium bromide homodimer (EthD-1), which causes dead cells to fluoresce orange (false-colored red). The sample in the first row was dehydrated and imaged by SEM (bottom row). Cells were manually counted from the raw *z*-stack confocal images, and the bars at the bottom represent the average and standard deviation from at least three independently prepared samples for each condition.

cationic PAH layer and the anionic CNCs are responsible for the excellent stability of these coatings.

Despite the simplicity of this method, some obstacles were encountered when coating 3D hydrogel scaffolds. Compared to DS3000, coating 3D printed PEG-DA structures using this procedure was more challenging as the small hydrogels were delicate, exhibited high water retention, and were easily detachable from the substrate. As a result, the numerous coating, washing, and drying steps involved required careful handling of samples and avoiding harsh drying methods such as the use of an air gun. As previously discussed, a key step to obtaining uniform and reproducible coatings was thoroughly washing away excess PAH, which would otherwise result in the formation of aggregate cellulose fibers and films. Achieving this required an intermediary drying step between washing, which we suspect is necessary for the PAH chains to collapse onto the PEG-DA scaffold to irreversibly coat it. This requirement may pose issues when coating more delicate scaffolds, where the process of dehydration could significantly deform or collapse fine structures.

2.4. Impact of CNC Coatings on Cellular Attachment and Morphology. The impact of CNC coatings and their density on the adhesion and morphology of PC3-GFP human prostate cancer cells was studied on PEG-DA and DS3000 3D printed scaffolds. In the absence of CNCs, PC3 cells did not adhere to PEG-DA woodpiles (2 ± 2 bound cells/scaffold), as seen by spinning-disk confocal microscopy (Figure 5). In contrast, coating the scaffold with CNCs using a 30 ppm solution caused some cells to bind to the PEG-DA hydrogel (35 ± 14 cells/scaffold) and a high coating concentration of 3000 ppm resulted in complete coverage of the woodpile with cells (97 ± 13 cells/scaffold). As seen in the fluorescence orthogonal projections and scanning electron microscopy (SEM) micrographs, the cells were able to reside deep within the woodpile

https://doi.org/10.1021/acsabm.1c00970
ACS Appl. Bio Mater. 2021, 4, 8443−8455

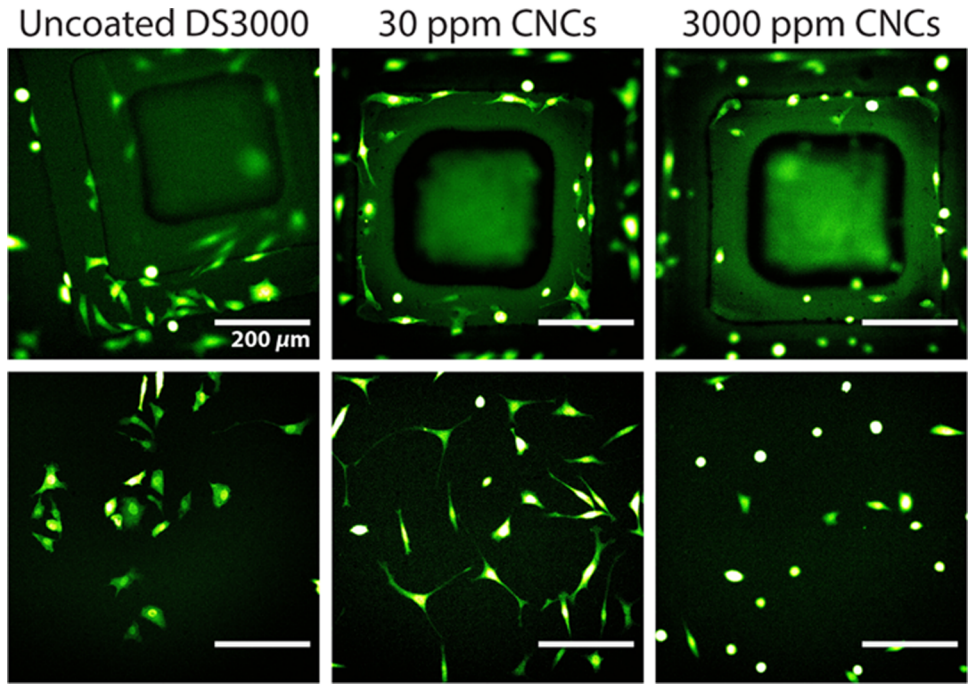

Figure 6. Epifluorescence images of PC3-GFP cells cultured on DS3000 2.5D pyramids. Cells were seeded at a density of 15 000 cells/cm^2 for 1 h, supplemented with media, and cultured for 3 days. Live-cell images were acquired in the green channel using an epifluorescence microscope at room temperature. The top row consists of representative images of cells adhering to the pyramid while the images in the bottom row were acquired on the flat part of the DS3000 pyramid array.

and occasionally suspended between beams when not lying flat or wrapping them. Staining with ethidium bromide homodimer (EthD-1) did not result in red fluorescence from any of the cells, indicating that CNCs did not hinder cellular viability at both high and low coating concentrations after 2 days of cell culture. Unexpectedly, this dye was able to nonspecifically stain CNCs and in this case highlighted the scaffold coating with a fluorescence intensity that was proportional to the density of CNCs.

Coating PEG-DA with CNCs permitted attachment of the PC3 cells to the 3D scaffold in a fashion that could be tuned by controlling the surface density of CNCs. The ability of these nanoparticles to enhance the attachment of PC3 cells to PEG-DA, which was also observed with 2.5D structures (Figure S5), is not fully understood, but we hypothesize that it arises from the presence of nanotopography, from the increased hydrophobicity of the CNCs, and from the higher local stiffness introduced by the rigid nanoparticles. The coverage of the hydrogel surface with CNCs may mask the protein-repelling properties of PEG-DA and in turn allow adhesion proteins, which are present in media and on the cellular surface, to attach to the scaffold. This effect may be complemented by the chemical properties of the CNC surface, which presents both hydrophobic and hydrophilic facets that potentially act as adhesion sites for the cells.[46,47] Additionally, nanotopography and the increase in surface roughness introduced by the CNCs, which have been previously shown to significantly enhance cellular adhesion, may provide more features for the cells to interact with and adhere to.[48−50] The possibility of PAH being responsible for the enhanced cellular adhesion was ruled out with a control experiment on 2.5D PEG-DA structures coated only with PAH, where cells could not bind to the hydrogel (Figure S5). The concentration of PAH also remained constant when the woodpiles were coated with 30 or 3000 ppm CNCs, while the observed cellular adhesion was dependent on the concentration of the CNC coating. Thus, it can be concluded that the enhanced adhesion was a direct result of the presence of CNCs.

Similar enhancements in cell binding were not observed for DS3000 scaffolds coated with CNCs (Figure 6). This material is designed to be biocompatible and supported culturing of PC3 prostate cancer cells without any coatings. However, coating 2.5D DS3000 scaffolds with CNCs altered the morphology of PC3 cells. In uncoated scaffolds, PC3 cells appeared to organize in clusters and lay flat on the surface while adopting epithelial-like, polygon-shaped morphologies. Upon sparsely coating the scaffold with CNCs (30 ppm), the cells were more uniformly distributed along the scaffold and adopted elongated, multipolar configurations that are reminiscent of fibroblasts and similar to those adopted by PC3 cells cultured on control glass surfaces (Figure S6). When the scaffolds were densely coated with CNCs (3000 ppm), most of the cells were spherical and exhibited little to no cellular extensions. Similar trends in morphology were observed with PC3 cells cultured on 3D PEG-DA scaffolds densely coated with CNCs (Figures 5 and S5). However, it is difficult to make a comparison to pristine PEG-DA as little to no cells adhered. Given the propensity of PC3 cells to adhere to CNCs, as seen with coated PEG-DA, their morphology appeared to be dictated by the amount of CNCs present within their surroundings. With a moderate CNC density, the cells extended filipodia to sites where CNCs are present, giving rise to their elongated morphology. When the scaffold surface was densely covered with CNCs, the cells did not extend to other areas and retained a circular morphology. This could be the result of excessive nanotopography, resulting in a poor cell condition (despite the fact that they did not stain red with ethidium bromide homodimer), which highlights the importance of nanotopography not only on adhesion but also on cell phenotype. Thus, by tuning the density of CNCs present on the

https://doi.org/10.1021/acsabm.1c00970
ACS Appl. Bio Mater. 2021, 4, 8443−8455

scaffold surface, it was possible to alter the adhesion and phenotype adopted by PC3 prostate cancer cells when cultured on DS300 and PEG-DA. In future work, this can be complemented with metabolic assays and biochemical functionalization of the scaffolds to assess cellular fitness and further recapitulate real cell microenvironments to guide the differentiation of cells to specific lineages. On the other hand, the control offered by CNC coatings on the adhesion of PC3 cells to PEG-DA scaffolds can be used for the development of medical devices that isolate rare circulating tumor cells from the blood.

3. CONCLUSIONS

The process of additive manufacturing through single- and two-photon polymerization 3D printing systems allowed the fabrication of PEG-DA and DS3000 scaffolds with precise control on their size, hierarchy, and geometric complexity. We have extended the method of layer-by-layer polyelectrolyte dip coating with CNCs to introduce nanostructured topography and chemical functionality onto the surface of 3D printed structures in a tunable and versatile fashion. Coating the scaffolds with various densities of CNCs enabled control on the adherence of GFP-PC3 prostate cancer cells to PEG-DA surfaces and altered the phenotype of the cells when cultured on both PEG-DA and DS3000 structures. The mechanism by which CNCs influence the attachment and morphology of these cells remains unclear as it is challenging to decouple the effects of surface nanoroughness and surface chemistry that are simultaneously introduced by the CNCs. The versatility offered by biotin-CNCs in functionalizing scaffolds with streptavidin-conjugated molecules allows future exploration on using biochemical factors to further mimic real cellular microenvironments. Fabricating realistic cellular scaffolds would promote the desirable cellular behavior that is necessary to study fundamental biological concepts and create artificial tissues, organoid models, and medical devices.

4. EXPERIMENTAL SECTION

4.1. Materials. 3-(Trimethoxysilyl)propyl methacrylate (98%, TPM), poly(ethylene glycol)diacrylate (PEG-DA, M_n = 700 Da, n = 1.47), diphenyl(2,4,6-trimethylbenzoyl)phosphine oxide (Irgacure 819), Triton X-100, 10% formalin, 4% glutaraldehyde, 99% acetic acid, poly(ethylene glycol) (PEG, M_w = 1050 Da), triethylamine (Et_3N), 4-dimethylaminopyridine (DMAP), p-toluene sulfonylchloride, sodium sulfate (NA_2SO_4), copper sulfate pentahydrate ($CuSO_4 \cdot 5H_2O$), ascorbic acid, cyanuric chloride, propargylamine, sodium hydroxide (NaOH), potassium carbonate (K_2CO_3), N-hydroxysuccinimide, dicyclohexylcarbodiimide (DCC), and biotinyl-N-hydroxysuccinimide were purchased from Sigma-Aldrich (Oakville, Ontario, Canada). The DS3000 negative tone resist was purchased from DWS Systems (Italy). Poly(allylamine hydrochloride) (PAH, M_w = 120 000−200 000 Da) was purchased from Polysciences (Warrington, PA) and stored at −20 °C. Sulfo-Cyanine5 azide was purchased from Lumiprobe Corp. (Hunt Valley, MD). Poly(ethylene glycol) monoallyl ether (M_w = 388 Da) was a gift from EnRoute Interfaces, Inc. (Hamilton, ON, Canada). Cellulose nanocrystals (CNCs, spray-dried), were kindly donated by CelluForce Inc. (Montreal, QC, Canada) and were previously characterized by dynamic light scattering, atomic force microscopy, and X-ray diffraction to have an average hydrodynamic radius of 70 ± 3 nm, a ζ-potential of −39 ± 1 mV, length of 180 ± 90 nm, cross section of 6 ± 2, and crystallinity of 90%, respectively.[51] All mentions of water refer to double-distilled 18.2 MΩ water (ddH_2O, ultrapure, type I), generated from a Milli-Q direct purifier system (Millipore Sigma). Cy5-conjugated streptavidin (0.1 mg/mL in phosphate-buffered saline, PBS with 4 mg/mL bovine serum albumin, BSA), Gibco Dulbecco's modified Eagle medium (DMEM) (high glucose, GlutaMAX supplement, pyruvate), Gibco penicillin−streptomycin, Gibco fetal bovine serum, and Gibco geneticin were purchased from Thermo Fisher Scientific (Mississauga, Ontario, Canada). Human prostate cancer cells (PC3), which were transformed to constitutively express the green fluorescent protein in their cytoplasm (PC3-GFP), were kindly provided by the Cuvillier Laboratory at the Institute of Pharmacology and Structural Biology (IPBS, Toulouse, France).

4.2. Functionalization of CNCs with Cy5 and Biotin. CNCs were functionalized with Cy5 or biotin using triazine click-chemistry using methods adapted from our previous work.[33,52] Since trichlorotriazine presents a substitution site at each chlorine, grafting this molecule onto the CNC surface hydroxyl groups allows it to be used as a linker when other sites are reacted with the functionality of interest. A general implementation of this involved appending, to the triazine linker, a group that can participate in a click-reaction with a molecule of interest that presents a complementary chemical handle. Many widely used functionalities, such as dyes and ligands, are commercially available with chemical handles that are compatible with click-reactions. CNCs were grafted with: (i) dichlorotriazine propargylamine, which was then reacted with sulfo-Cy5 azide, or (ii) chlorotriazine azido-PEG-allyl-PEG, to which alkyne-biotin was then conjugated (Scheme S1). The second linker also possesses an alkene group, which could be used to functionalize the CNCs with molecules bearing a thiol moiety. The synthesis of the triazine linkers and alkyne-biotin (Scheme S2), and their subsequent grafting onto CNCs are outlined in the Supporting Information.

4.3. Silanization of Glass Coverslips and Indium-Tin-Oxide (ITO)-Coated Slides. Glass substrates were silanized with a methacrylate group to ensure the proper adhesion of spin-coated thin films. Circular glass coverslips (No. 1.5, 18 mm diameter, 170 μm nominal thickness, VWR, Mississauga, Ontario, Canada) or indium-tin-oxide (ITO)-coated glass slides (25 mm × 25 mm, 0.7 mm thickness, Nanoscribe GMBH, Karlsruhe, Germany) were sequentially cleaned with acetone, ethanol, and water and then dried with an air gun. The glass or ITO surface was activated with a Diener Electronic air plasma machine (5 min, 0.6 mbar, 30 W) immediately before drop-casting TPM (2% v/v in water with 0.1% v/v of acetic acid) over the substrates. The droplets of the TPM solution were kept for 2 h before rinsing the substrates with ethanol and water and then drying with an air gun.

4.4. Spin-Coating Thin Films of PEG-DA and DS3000 on Circular Glass Substrates. DS3000 was spin-coated onto silanized 18 mm glass slides (5000 rpm, 60 s, 1000 rpm/s) using a Suss MicroTec spin-coater (Karl Suss, Garching, Germany) and cured immediately with a flood exposure of 405 nm light (60 s, 30 mW/cm^2) using a Suss MicroTec MA/BA6 mask aligner (Karl Suss, Garching, Germany). The samples were rinsed in ethanol for 10 s and then dried with an air gun. PEG-DA thin films were prepared the same way but on DS3000-coated glass coverslips to improve adhesion.

4.5. 3D Printing DS3000 Using Single-Photon Polymerization. DS3000 structures were fabricated using laser-assisted stereolithography; a DWS 029J+ 3D-printer from DWS Systems equipped with a 405 nm laser (86 mW, Solid State BluEdge BE-1800C) and a galvanometric mirror that can achieve a maximum scanning speed of 6000 mm/s. To ensure proper adhesion of the samples to the printer platform, the first four layers were overexposed by reducing the scanning speed to 200 mm/s, whereas the rest of the structures were printed at 3000 mm/s. The hatching and slicing distances were set to 40 μm and 50 μm, respectively. The 2.5D pyramids, which consisted of three, 50 μm high steps with side lengths of 700, 500, and 300 μm, were printed as an array on a circular base with a diameter of 20 and 2 mm thickness. The 3D bone scaffold was printed from a digital reconstruction model that was generated using propagation phase-contrast synchrotron microtomography of a trabecular bone within a horse femoral epiphysis, as described in previous work.[39] 3D printed samples were then developed in an ethanol bath under sonication for 15 min to remove the nonpolymerized material. Afterward, the samples were air-dried and flood exposed to UV light to ensure complete cross-linking of the resin.

4.6. 3D Printing PEG-DA Using Two-Photon Polymerization Direct Laser Writing. PEG-DA structures were 3D printed by two-photon polymerization (2PP) direct laser writing using a Nanoscribe

https://doi.org/10.1021/acsabm.1c00970
ACS Appl. Bio Mater. 2021, 4, 8443−8455

Photonic Professional GT2 (Karlsruhe, Germany) system similar to previous work.[42] Briefly, PEG-DA 700 was thawed (from −20 °C) for an hour at room temperature (rt), combined with the photoinitiator Irgacure 819 to a concentration of 0.5% w/w and stirred for 3 h in the dark. Water was added to make a 3:1 PEG-DA/water solution and stirred overnight at rt in the dark. Silanized ITO glass slides were coated with DS3000, using the same procedure as above, to improve the adhesion of PEG-DA to the substrate and allow the microscope to find the substrate interface. The substrate was fixed onto a dip-in laser lithography holder and a droplet of the PEG-DA solution was placed in the center. The holder was inverted and mounted onto the stage of the Nanoscribe. In such a configuration, the employed 2PP objective is directly immersed in the photosensitive liquid. The 2PP setup system consisted of an inverted two-photon Carl Zeiss microscope, coupled to a 780 nm femtosecond pulsed fiber laser (100 fs, 50 mW, FemtoFiber Pro, Toptica Photonics), with a resonating scanner and a galvanometric mirror system allowing a moving-beam fixed-sample configuration. The sample was approached with a 25× (NA 0.8) water-immersion objective, with the collar set a quarter way from the glycerol mark to the watermark, until the lens was in immersion with the resin, and the interface between the substrate and the photosensitive PEG-DA interface was found. The structures of interest were designed beforehand using CAD software Autodesk Fusion 360 and imported as a work file into Nanoscribe with both the hatching and slicing distance writing parameters equal to 400 nm. The 2.5D pillar array design, which consisted of a 300 μm × 300 μm × 15 μm base, half-covered with 5 μm diameter pillars, 10 μm apart, was printed with a writing speed of 25 mm/s and a nominal laser power of 70%. The 3D woodpile design (270 μm × 270 μm × 280 μm) consisted of perpendicularly stacked layers, each composed of 20 μm diameter cylinders interspaced 50 μm apart. This structure was printed three times on each sample with a writing speed of 50 mm/s and different laser powers (78, 79, and 80%) to produce scaffolds with various structural integrities, stiffness, and adhesion to the substrate (Figure S1B). The 3D printed structures were developed in two water baths for 30 min each. No differences in the coating were observed between the samples fabricated using different laser powers.

4.7. Dip-Coating Thin Films and 3D Printed Structures with CNCs. Spray-dried CNCs were dissolved in water to make a 3 wt % (30 000 ppm) suspension through repeated cycles of vortex mixing and dispersion with a VC334 Vibracell point probe sonicator (100 W, 2 s pulses, 6 min with a 3 mm tapered microtip) until it was clear. Through serial dilutions of this solution, 3000−3 ppm CNC suspensions were prepared and dispersed with point probe sonication after each dilution. To dip-coat structures with CNCs, it was first necessary to coat them with PAH, which was prepared from powder form to make a 1 wt % solution. The PAH solution was used within 2 weeks, while all of the CNC solutions with a concentration lower than 3000 ppm were prepared fresh each time as they could be significantly depleted with each coating.

To ensure adequate wettability, 3D printed DS300 structures were first activated with air plasma (30 s, 0.6 mbar, 30 W). 3D printed PEG-DA structures were not plasma-activated as they were stored in water after printing to avoid collapse of the hydrogel. The samples were then "dipped", or placed, into a plastic petri dish containing 20 mL of PAH for 15 min. To wash off excess PAH, the samples were washed in two steps by placing them in a water dish for 10 min, air drying, and then washing in another water dish for 10 min. Samples that were washed in one step only involved submersion in a water dish for 10 min and then air drying. The structures were then dipped into a 20 mL solution of CNCs for 15 min, washed in a water dish for 10 min, and air-dried. Thin films and 3D printed DS3000 samples could be dried using an air gun, while PEG-DA structures were left to gradually dry at rt as they could easily detach from the substrate in the presence of strong airflow.

4.8. Functionalization of 3D Scaffolds. Three-dimensional (3D) structures were coated using the dip-coating method with a layer of CNCs, 10% of which were functionalized with either Cy5 or biotin. For postcoating functionalization, the PEG-DA woodpile scaffold was incubated with 100 μL of 0.01 mg/mL Cy5-streptavidin in PBS for 30 min within a Pyrex cloning cylinder and then washed for 30 min in PBS.

4.9. Culture of PC3-GFP Prostate Cancer Cells. A 1.5 cm × 1.5 cm frame cut from double-sided adhesive tape (0.25 mm thick, Thermo Fisher) was placed on the center of a glass substrate containing 3D printed PEG-DA structures. The samples were placed in a Petri dish and sterilized with 70% ethanol for 30 min, rinsed with PBS, and 300 μL of PC3-GFP cells were seeded within the frame (to confine the seeding area and minimize the number of cells used during the inoculation step) at a density of 10 000 cells/cm^2 and incubated for 1 h (37 °C, 5% CO_2). The cells were supplemented with media (2 mL of DMEM with 10% FBS, 1% penicillin/streptomycin, and 1% geneticin) and cultured for 1 or 2 days on the 2.5D or 3D structures, respectively. DS3000 2.5D structures were cultured with PC3-GFP cells in a similar fashion, but an additional washing step of 2 days in PBS was done before dip coating and cell culture. The structures, without a frame, were placed in a 6-well cell culture plate (Flat Bottom, Corning Costar), seeded with 15 000 cells/cm^2, and cultured for 3 days.

Cells cultured on 2.5D DS3000 or PEG-DA structures (Figures 6 and S5) were imaged live, without staining or fixation. Cells cultured on 3D PEG-DA woodpile structures (Figure 5a) were fixed with 10% formalin for 30 min, permeabilized with 0.2% Triton X-100 for 3 min, and stained for actin and nuclear DNA with rhodamine−phalloidin (Invitrogen, 16.5 mg/mL, 30 min, rt) and DAPI (Invitrogen, 10 μg/mL, 15 min, rt), respectively. The stained samples were stored in PBS, in the dark at 4 °C until they were imaged. To test for the presence of dead cells, duplicate samples were stained with 4 μM ethidium bromide homodimer (Live/Dead kit for mammalian cells, Invitrogen) for 30 min at 37 °C. After fluorescence imaging, this sample was then fixed with 4% glutaraldehyde (in PBS) for 4 h, washed once with PBS (4 min), three times with water (2 min each), dehydrated with consecutive ethanol baths (50, 70, 90, and 100% in PBS for 4 min per bath), washed with 100% ethanol twice (2 min each) and then gradually air-dried at rt before imaging with SEM (Figure 5c).

4.10. Characterization of the Surface Roughness and CNC Coating Density with AFM. The nanostructure and roughness arising from the CNC coating process and its response to variations in CNC concentrations were assessed using a Bruker ICON AFM. All images were acquired in tapping mode with a Bruker FESP cantilever of a spring constant of 1−5 N/m and a resonating frequency of 72 kHz. Areas of 2.5 μm × 2.5 μm were scanned at three or more random locations on each thin film, the flat side of the PEG-DA 2.5D pillar arrays, or the top of the DS3000 pyramids, with 256 lines at a rate of 0.5 lines/s. Image correction, including plane leveling and row alignment, and analysis were performed with Gwydion 2.47. RMS roughness, S_q, was calculated by this software using the following formula, where z_n and $\bar{z}$ represent the height and mean height, respectively

$$S_q = \sqrt{\frac{1}{N}\sum_{n=1}^{N}(z_n - \bar{z})^2}$$

4.11. Laser Scanning Confocal Microscopy Imaging of Scaffolds Coated with Functionalized CNCs. The functionalization of 3D printed structures with Cy5 was characterized in terms of coverage and density using a Leica SP8 DM6000CS laser scanning confocal microscope. All samples were excited with a 638 nm, 30 mW, diode laser (LASOS, Jena, Germany), and fluorescence was collected with a spectral photomultiplier tube detector (Hamamatsu R6357, Hamamatsu City, Shizuoka, Japan) set to an emission band of 730−800 nm. Images of PEG-DA woodpile structures were acquired using LAS X software with a 20×/NA 0.7 water-immersion objective using *xy*- and *z*-steps of 0.45 and 1.2 μm, respectively. Laser power compensation, where higher laser intensities were used at deeper sections, was employed in an attempt to completely visualize the structure. DS3000 bone scaffolds were imaged similarly, however, given their centimeter sizes, it was not possible to image them in their entirety. To this end, images of the control and coated samples were all acquired using the same conditions, where 1.5 mm × 1.5 mm × 0.75 mm sections were captured using a 10×/NA 0.3 air objective, 10% laser power, and *xyz*-steps of 3 μm. Orthogonal projections and 3D renders were produced with ImageJ software.

https://doi.org/10.1021/acsabm.1c00970
ACS Appl. Bio Mater. 2021, 4, 8443−8455

4.12. Spinning-Disk Confocal Imaging of PC3 Cancer Cells on PEG-DA 3D Woodpiles. Cells cultured on 3D scaffolds were imaged using a Leica DMI8 inverted microscope controlled using imaging software ImageJ MicroManager and equipped with Yokogawa CSU-X1 spinning-disk confocal, 405 nm and 488 nm diode, 100 mW lasers, and a 561 nm, diode-pumped solid-state 100 mW laser. Emitted light was collected with a 50 μm Nipkow disk spinning at 5000 rpm before being filtered with a 450/50 nm, 525/50 nm, or 595/50 nm bandpass filter and captured with a Flash4.0 v3 Hamamatsu camera. The samples were inverted and mounted onto a No. 1.5 glass coverslip with a 0.25 mm thick double-sided sticky frame to create an aqueous chamber of cell medium and allow imaging with the inverted microscope. Images were captured using a 10×/NA 0.45 water-immersion objective using an exposure of 200 ms and 2 μm z-steps. Cell counting was done manually using the multipoint tool in ImageJ.

4.13. Epifluorescence Imaging of PC3s on 2.5D DS3000 and PEG-DA Structures. PC3-GFP cells were imaged with an Olympus BX51 upright epifluorescence microscope using a 10× NA 0.3 objective and an X-Cite 120 lamp. Emitted light was filtered through a 545/55 nm bandpass filter and captured with a Hamamatsu C13440 ORCA-Flash4.0 CMOS digital camera controlled by imaging software ImageJ MicroManager.

4.14. SEM Characterization of 3D Printed Structures. Three-dimensional (3D) printed samples were imaged through secondary electron emission with a Hitachi S-4800 system set to a working accelerating voltage and a current of 0.7 kV and 10 μA, respectively, at a distance of 12.8 mm.

■ ASSOCIATED CONTENT

Supporting Information

The Supporting Information is available free of charge at https://pubs.acs.org/doi/10.1021/acsabm.1c00970.

List of synthetic procedures and schemes of linkers and their grafting onto cellulose nanocrystals; AFM, SEM, and fluorescence results of various control experiments regarding the impact of PAH coating and its washing on CNC coating and cell adherence; and thorough topographical and roughness analysis of CNC coatings and 3D rendered confocal fluorescence images (PDF)

■ AUTHOR INFORMATION

Corresponding Author

Jose Moran-Mirabal − *Department of Chemistry and Chemical Biology, Centre for Advanced Light Microscopy, and Brockhouse Institute for Materials Research, McMaster University, Hamilton, Ontario L8S 4M1, Canada;* orcid.org/0000-0002-4811-3085; Email: mirabj@mcmaster.ca

Authors

Mouhanad Babi − *Department of Chemistry and Chemical Biology, McMaster University, Hamilton, Ontario L8S 4M1, Canada*

Roberto Riesco − *LAAS-CNRS, Université Toulouse III—Paul Sabatier, 31400 Toulouse, France*

Louisa Boyer − *LAAS-CNRS, Université Toulouse III—Paul Sabatier, 31400 Toulouse, France*

Ayodele Fatona − *Department of Chemistry and Chemical Biology, McMaster University, Hamilton, Ontario L8S 4M1, Canada*

Angelo Accardo − *Department of Precision and Microsystems Engineering, Delft University of Technology, 2628 CD Delft, Netherlands;* orcid.org/0000-0003-0442-3652

Laurent Malaquin − *LAAS-CNRS, Université Toulouse III—Paul Sabatier, 31400 Toulouse, France;* orcid.org/0000-0003-4791-3352

Complete contact information is available at: https://pubs.acs.org/10.1021/acsabm.1c00970

Author Contributions

The manuscript was written through contributions of all authors. All authors have given approval to the final version of the manuscript.

Notes

The authors declare no competing financial interest.

■ ACKNOWLEDGMENTS

M.B. was supported through the Natural Sciences and Engineering Research Council (NSERC) of Canada Graduate Scholarship—Doctoral Award. J.M.-M. is the Tier 2 Canada Research Chair in Micro and Nanostructured Materials and the recipient of an Early Researcher Award from the Ontario Ministry of Research and Innovation. This work was supported by funding through a Discovery Grant from NSERC to JMM (RGPIN-2019-06433) and by the French RENATECH network. This research was partly supported as part of the MultiFAB project funded by FEDER European Regional Funds and French Région Occitanie (grant agreement number 16007407/MP0011594) and by the HoliFAB project funded by the European Union's Horizon 2020 Research and Innovation Program (grant agreement No. 760927). This research made use of instrumentation within McMaster's Centre for Advanced Light Microscopy.

■ ABBREVIATIONS

CNCs, cellulose nanocrystals; AFM, atomic force microscopy; ECM, extracellular matrix; PEG-DA, poly(ethylene glycol)-diacrylate; NPs, nanoparticles; LbL, layer-by-layer; PAH, poly(allylamine hydrochloride); PC3, human prostate cancer cells; GFP, green fluorescence protein; ITO, indium-tin-oxide; 2PP, two-photon polymerization; EthD-1, ethidium bromide homodimer; TPM, 3-(trimethoxysilyl)propyl methacrylate; Irgacure 819, diphenyl(2,4,6-trimethylbenzoyl)phosphine oxide; DMAP, 4-dimethylaminopyridine; NHS, *N*-hydroxysuccinimide; DCC, dicyclohexylcarbodiimide

■ REFERENCES

(1) Inzana, J. A.; Olvera, D.; Fuller, S. M.; Kelly, J. P.; Graeve, O. A.; Schwarz, E. M.; Kates, S. L.; Awad, H. A. 3D Printing of Composite Calcium Phosphate and Collagen Scaffolds for Bone Regeneration. *Biomaterials* **2014**, *35*, 4026−4034.

(2) Hockaday, L. A.; Kang, K. H.; Colangelo, N. W.; Cheung, P. Y. C.; Duan, B.; Malone, E.; Wu, J.; Girardi, L. N.; Bonassar, L. J.; Lipson, H.; Chu, C. C.; Butcher, J. T. Rapid 3D Printing of Anatomically Accurate and Mechanically Heterogeneous Aortic Valve Hydrogel Scaffolds. *Biofabrication* **2012**, *4*, No. 035005.

(3) Li, K.; Wang, D.; Zhao, K.; Song, K.; Liang, J. Electrohydrodynamic Jet 3D Printing of PCL/PVP Composite Scaffold for Cell Culture. *Talanta* **2020**, *211*, No. 120750.

(4) Yi, T.; Huang, S.; Liu, G.; Li, T.; Kang, Y.; Luo, Y.; Wu, J. Bioreactor Synergy with 3D Scaffolds: New Era for Stem Cells Culture. *ACS Appl. Bio Mater.* **2018**, *1*, 193−209.

(5) Kim, D. H.; Provenzano, P. P.; Smith, C. L.; Levchenko, A. Matrix Nanotopography as a Regulator of Cell Function. *J. Cell Biol.* **2012**, 351−360.

(6) Krishna, L.; Dhamodaran, K.; Jayadev, C.; Chatterjee, K.; Shetty, R.; Khora, S. S.; Das, D. Nanostructured Scaffold as a Determinant of Stem Cell Fate. *Stem Cell Res. Ther.* **2016**, 1−12.
(7) Yim, E. K. F.; Leong, K. W. Significance of Synthetic Nanostructures in Dictating Cellular Response. *Nanomedicine* **2005**, *1*, 10−21.
(8) Canty, E. G.; Lu, Y.; Meadows, R. S.; Shaw, M. K.; Holmes, D. F.; Kadler, K. E. Coalignment of Plasma Membrane Channels and Protrusions (Fibropositors) Specifies the Parallelism of Tendon. *J. Cell Biol.* **2004**, *165*, 553−563.
(9) Baselt, D. R.; Revel, J. P.; Baldeschwieler, J. D. Subfibrillar Structure of Type I Collagen Observed by Atomic Force Microscopy. *Biophys. J.* **1993**, *65*, 2644−2655.
(10) Provenzano, P. P.; Keely, P. J. Mechanical Signaling through the Cytoskeleton Regulates Cell Proliferation by Coordinated Focal Adhesion and Rho GTPase Signaling. *J. Cell Sci.* **2011**, *124*, 1195−1205.
(11) Dickinson, R. B.; Guido, S.; Tranquillo, R. T. Biased Cell Migration of Fibroblasts Exhibiting Contact Guidance in Oriented Collagen Gels. *Ann. Biomed. Eng.* **1994**, *22*, 342−356.
(12) Provenzano, P. P.; Inman, D. R.; Eliceiri, K. W.; Trier, S. M.; Keely, P. J. Contact Guidance Mediated Three-Dimensional Cell Migration Is Regulated by Rho/ROCK-Dependent Matrix Reorganization. *Biophys. J.* **2008**, *95*, 5374−5384.
(13) Wang, W.; Wyckoff, J. B.; Frohlich, V. C.; Oleynikov, Y.; Hüttelmaier, S.; Zavadil, J.; Cermak, L.; Bottinger, E. P.; Singer, R. H.; White, J. G.; Segall, J. E.; Condeelis, J. S. Single Cell Behavior in Metastatic Primary Mammary Tumors Correlated with Gene Expression Patterns Revealed by Molecular Profiling. *Cancer Res.* **2002**, *62*, 6278−6288.
(14) Abrams, G. A.; Goodman, S. L.; Nealey, P. F.; Franco, M.; Murphy, C. J. Nanoscale Topography of the Basement Membrane Underlying the Corneal Epithelium of the Rhesus Macaque. *Cell Tissue Res.* **2000**, *299*, 39−46.
(15) Liliensiek, S. J.; Nealey, P.; Murphy, C. J. Characterization of Endothelial Basement Membrane Nanotopography in Rhesus Macaque as a Guide for Vessel Tissue Engineering. *Tissue Eng., Part A* **2009**, *15*, 2643−2651.
(16) Karuri, N. W.; Liliensiek, S.; Teixeira, A. I.; Abrams, G.; Campbell, S.; Nealey, P. F.; Murphy, C. J. Bilogical Length Scale Topography Enhances Cell-Substratum Adhesion of Human Corneal Epithelial Cells. *J. Cell Sci.* **2004**, *117*, 3153−3164.
(17) Dalby, M. J.; Riehle, M. O.; Sutherland, D. S.; Agheli, H.; Curtis, A. S. G. Changes in Fibroblast Morphology in Response to Nano-Columns Produced by Colloidal Lithography. *Biomaterials* **2004**, *25*, 5415−5422.
(18) Lee, M. R.; Kwon, K. W.; Jung, H.; Kim, H. N.; Suh, K. Y.; Kim, K.; Kim, K. S. Direct Differentiation of Human Embryonic Stem Cells into Selective Neurons on Nanoscale Ridge/Groove Pattern Arrays. *Biomaterials* **2010**, *31*, 4360−4366.
(19) Teixeira, A. I.; Abrams, G. A.; Bertics, P. J.; Murphy, C. J.; Nealey, P. F. Epithelial Contact Guidance on Well-Defined Micro- and Nanostructured Substrates. *J. Cell Sci.* **2003**, *116*, 1881−1892.
(20) Lee, C. H.; Shin, H. J.; Cho, I. H.; Kang, Y. M.; Kim, I. A.; Park, K. D.; Shin, J. W. Nanofiber Alignment and Direction of Mechanical Strain Affect the ECM Production of Human ACL Fibroblast. *Biomaterials* **2005**, *26*, 1261−1270.
(21) Makaremi, S.; Luu, H.; Boyle, J. P.; Zhu, Y.; Cerson, C.; Bowdish, D. M. E.; Moran-Mirabal, J. M. The Topography of Silica Films Modulates Primary Macrophage Morphology and Function. *Adv. Mater. Interfaces* **2019**, *6*, No. 1900677.
(22) Melchels, F. P. W.; Feijen, J.; Grijpma, D. W. A Review on Stereolithography and Its Applications in Biomedical Engineering. *Biomaterials.* **2010**, *31*, 6121−6130.
(23) Zhang, S.; Ou, Q.; Xin, P.; Yuan, Q.; Wang, Y.; Wu, J. Polydopamine/Puerarin Nanoparticle-Incorporated Hybrid Hydrogels for Enhanced Wound Healing. *Biomater. Sci.* **2019**, *7*, 4230−4236.
(24) Guillaume, O.; Geven, M. A.; Sprecher, C. M.; Stadelmann, V. A.; Grijpma, D. W.; Tang, T. T.; Qin, L.; Lai, Y.; Alini, M.; de Bruijn, J. D.; Yuan, H.; Richards, R. G.; Eglin, D. Surface-Enrichment with Hydroxyapatite Nanoparticles in Stereolithography-Fabricated Composite Polymer Scaffolds Promotes Bone Repair. *Acta Biomater.* **2017**, *54*, 386−398.
(25) Tang, Y.; Zhao, Y.; Wang, X.; Lin, T. Layer-by-Layer Assembly of Silica Nanoparticles on 3D Fibrous Scaffolds: Enhancement of Osteoblast Cell Adhesion, Proliferation, and Differentiation. *J. Biomed. Mater. Res., Part A* **2014**, *102*, 3803−3812.
(26) Lee, J. H.; Lee, J. Y.; Yang, S. H.; Lee, E. J.; Kim, H. W. Carbon Nanotube-Collagen Three-Dimensional Culture of Mesenchymal Stem Cells Promotes Expression of Neural Phenotypes and Secretion of Neurotrophic Factors. *Acta Biomater.* **2014**, *10*, 4425−4436.
(27) Hirata, E.; Uo, M.; Takita, H.; Akasaka, T.; Watari, F.; Yokoyama, A. Multiwalled Carbon Nanotube-Coating of 3D Collagen Scaffolds for Bone Tissue Engineering. *Carbon* **2011**, *49*, 3284−3291.
(28) Jung, Y.; Chung, Y. I.; Kim, S. H.; Tae, G.; Kim, Y. H.; Rhie, J. W.; Kim, S. H.; Kim, S. H. In Situ Chondrogenic Differentiation of Human Adipose Tissue-Derived Stem Cells in a TGF-B1 Loaded Fibrin-Poly(Lactide-Caprolactone) Nanoparticulate Complex. *Biomaterials* **2009**, *30*, 4657−4664.
(29) Engler, A. J.; Sen, S.; Sweeney, H. L.; Discher, D. E. Matrix Elasticity Directs Stem Cell Lineage Specification. *Cell* **2006**, *126*, 677−689.
(30) Moon, R. J.; Martini, A.; Nairn, J.; Simonsen, J.; Youngblood, J. Cellulose Nanomaterials Review: Structure, Properties and Nanocomposites. *Chem. Soc. Rev.* **2011**, *40*, 3941−3994.
(31) Habibi, Y.; Lucia, L. A.; Rojas, O. J. Cellulose Nanocrystals: Chemistry, Self-Assembly, and Applications. *Chem. Rev.* **2010**, *110*, 3479−3500.
(32) Gill, U.; Sutherland, T.; Himbert, S.; Zhu, Y.; Rheinstädter, M. C.; Cranston, E. D.; Moran-Mirabal, J. M. Beyond Buckling: Humidity-Independent Measurement of the Mechanical Properties of Green Nanobiocomposite Films. *Nanoscale* **2017**, *9*, 7781−7790.
(33) Fatona, A.; Berry, R. M.; Brook, M. A.; Moran-Mirabal, J. M. Versatile Surface Modification of Cellulose Fibers and Cellulose Nanocrystals through Modular Triazinyl Chemistry. *Chem. Mater.* **2018**, *30*, 2424−2435.
(34) Hu, H.; Yuan, W.; Liu, F.-S.; Cheng, G.; Xu, F.-J.; Ma, J. Redox-Responsive Polycation-Functionalized Cotton Cellulose Nanocrystals for Effective Cancer Treatment. *ACS Appl. Mater. Interfaces* **2015**, *7*, 8942−8951.
(35) Despres, H. W.; Sabra, A.; Anderson, P.; Hemraz, U. D.; Boluk, Y.; Sunasee, R.; Ckless, K. Mechanisms of the Immune Response Cause by Cationic and Anionic Surface Functionalized Cellulose Nanocrystals Using Cell-Based Assays. *Toxicol. In Vitro* **2019**, *55*, 124−133.
(36) Wan, W.; Ouyang, H.; Long, W.; Yan, W.; He, M.; Huang, H.; Yang, S.; Zhang, X.; Feng, Y.; Wei, Y. Direct Surface Functionalization of Cellulose Nanocrystals with Hyperbranched Polymers through the Anionic Polymerization for PH-Responsive Intracellular Drug Delivery. *ACS Sustainable Chem. Eng.* **2019**, *7*, 19202−19212.
(37) Domingues, R. M. A.; Gomes, M. E.; Reis, R. L. The Potential of Cellulose Nanocrystals in Tissue Engineering Strategies. *Biomacromolecules.* **2014**, 2327−2346.
(38) de France, K. J.; Badv, M.; Dorogin, J.; Siebers, E.; Panchal, V.; Babi, M.; Moran-Mirabal, J.; Lawlor, M.; Cranston, E. D.; Hoare, T. Tissue Response and Biodistribution of Injectable Cellulose Nanocrystal Composite Hydrogels. *ACS Biomater. Sci. Eng.* **2019**, *5*, 2235−2246.
(39) Moreau, C.; Beury, N.; Delorme, N.; Cathala, B. Tuning the Architecture of Cellulose Nanocrystal-Poly(Allylamine Hydrochloride) Multilayered Thin Films: Influence of Dipping Parameters. *Langmuir* **2012**, *28*, 10425−10436.
(40) Martin, C.; Jean, B. Nanocellulose/Polymer Multilayered Thin Films: Tunable Architectures towards Tailored Physical Properties. *Nord. Pulp Pap. Res. J.* **2014**, *29*, 19−30.
(41) Mézière, F.; Juskova, P.; Woittequand, J.; Muller, M.; Bossy, E.; Boistel, R.; Malaquin, L.; Derode, A. Experimental Observation of Ultrasound Fast and Slow Waves through Three-Dimensional Printed Trabecular Bone Phantoms. *J. Acoust. Soc. Am.* **2016**, *139*, No. EL13.

https://doi.org/10.1021/acsabm.1c00970
ACS Appl. Bio Mater. 2021, 4, 8443−8455

(42) Accardo, A.; Blatché, M. C.; Courson, R.; Loubinoux, I.; Vieu, C.; Malaquin, L. Two-Photon Lithography and Microscopy of 3D Hydrogel Scaffolds for Neuronal Cell Growth. *Biomed. Phys. Eng. Express* **2018**, *4*, No. 027009.
(43) de Mesquita, J. P.; Patrício, P. S.; Donnici, C. L.; Petri, D. F.; de Oliveira, L. C. A.; Pereira, F. V. Hybrid Layer-by-Layer Assembly Based on Animal and Vegetable Structural Materials: Multilayered Films of Collagen and Cellulose Nanowhiskers. *Soft Matter* **2011**, *7*, 4405−4413.
(44) Huang, C.; Fang, G.; Zhao, Y.; Bhagia, S.; Meng, X.; Yong, Q.; Ragauskas, A. J. Bio-Inspired Nanocomposite by Layer-by-Layer Coating of Chitosan/Hyaluronic Acid Multilayers on a Hard Nanocellulose-Hydroxyapatite Matrix. *Carbohydr. Polym.* **2019**, *222*, No. 115036.
(45) de France, K. J.; Babi, M.; Vapaavuori, J.; Hoare, T.; Moran-Mirabal, J.; Cranston, E. D. 2.5D Hierarchical Structuring of Nanocomposite Hydrogel Films Containing Cellulose Nanocrystals. *ACS Appl. Mater. Interfaces* **2019**, *11*, 6325−6335.
(46) Biermann, O.; Hädicke, E.; Koltzenburg, S.; Müller-Plathe, F.; Müller-Plathe, F.; Biermann, D.-C. O.; Hädicke, E.; Koltzenburg, S. Hydrophilicity and Lipophilicity of Cellulose Crystal Surfaces. *Angew. Chem., Int. Ed.* **2001**, *40*, 3822−3825.
(47) Mazeau, K. On the External Morphology of Native Cellulose Microfibrils. *Carbohydr. Polym.* **2011**, *84*, 524−532.
(48) Or, T.; Saem, S.; Esteve, A.; Osorio, D. A.; de France, K. J.; Vapaavuori, J.; Hoare, T.; Cerf, A.; Cranston, E. D.; Moran-Mirabal, J. M. Patterned Cellulose Nanocrystal Aerogel Films with Tunable Dimensions and Morphologies as Ultra-Porous Scaffolds for Cell Culture. *ACS Appl. Nano Mater.* **2019**, *2*, 4169−4179.
(49) Mo, Y.; Guo, R.; Liu, J.; Lan, Y.; Zhang, Y.; Xue, W.; Zhang, Y. Preparation and Properties of PLGA Nanofiber Membranes Reinforced with Cellulose Nanocrystals. *Colloids Surf., B* **2015**, *132*, 177−184.
(50) Liu, S.; Jin, M.; Chen, Y.; Gao, H.; Shi, X.; Cheng, W.; Ren, L.; Wang, Y. High Internal Phase Emulsions Stabilised by Supramolecular Cellulose Nanocrystals and Their Application as Cell-Adhesive Macroporous Hydrogel Monoliths. *J. Mater. Chem. B* **2017**, *5*, 2671−2678.
(51) Reid, M. S.; Villalobos, M.; Cranston, E. D. Benchmarking Cellulose Nanocrystals: From the Laboratory to Industrial Production. *Langmuir* **2017**, *33*, 1583−1598.
(52) de France, K. J.; Badv, M.; Dorogin, J.; Siebers, E.; Panchal, V.; Babi, M.; Moran-Mirabal, J.; Lawlor, M.; Cranston, E. D.; Hoare, T. Tissue Response and Biodistribution of Injectable Cellulose Nanocrystal Composite Hydrogels. *ACS Biomater. Sci. Eng.* **2019**, *5*, 2235−2246.

https://doi.org/10.1021/acsabm.1c00970
ACS Appl. Bio Mater. 2021, 4, 8443−8455